Evidence for Whole-Beam Self-Focusing of Induced Spatially Incoherent Laser Light in Large Underdense Plasma

T. Afshar-rad, L. A. Gizzi, M. Desselberger, F. Khattak, and O. Willi
The Blackett Laboratory, Imperial College of Science and Technology, Prince Consort Road, London SW7 2BZ, United Kingdom

A. Giulietti
Istituto di Fisica Atomica e Molecolare, Piza, Italy
(Received 16 September 1991)

The propagation of an intense electromagnetic pulse in a large underdense plasma has been investigated using spatially and temporally incoherent laser light. Spatial incoherence was obtained using the induced spatial incoherence (ISI) technique. The first observation of the occurrence of thermal whole-beam self-focusing with ISI laser light is presented. Thermal imaging with a multiframe x-ray camera (140 ps gate time) was used to record the propagation characteristics of the interaction beam through the plasma. A direct measurement of the self-focusing growth length has been made.

PACS numbers: 52.40.Db, 52.35.Mw, 52.40.Nk

A crucial requirement for direct-drive inertial confinement fusion is a high degree of irradiation uniformity at the pellet surface [1]. However, the strong tendency for high-power laser beams to self-focus in the large underdense plasmas surrounding such targets frustrates attempts to achieve this goal. This phenomenon usually manifests itself in the self-focusing of small-scale-length intensity nonuniformities, "hot spots," present in the spatial profile of the incident beam [2]. In addition, the subsequent increase in intensity can initiate other harmful instabilities such as stimulated Brillouin and Raman scattering [3]. Recent experimental results suggest that laser-beam "smoothing" using the induced spatial incoherence [4] (ISI) technique can be very effective in suppressing these instabilities [5]. With ISI, the far-field intensity distribution is an interference pattern which shifts on time scales of the order of the laser coherence time t_c, typically less than a few picoseconds. Since, in general, t_c is much less than the hydrodynamic response time of the plasma, the plasma should be insensitive to the large intensity modulations of the shifting interference pattern and respond instead to the smoothed time-average optical distribution. However, this profile is static and of finite size. As such, the incident beam itself can in effect behave as a large "hot spot" and become unstable to whole-beam self-focusing under suitable interaction conditions [6], and warrants investigation.

In this Letter a study is made of the interaction of a high-powered broadband ISI laser beam with a large preformed underdense "homogeneous" plasma. The first observation of the occurrence of thermal whole-beam self-focusing with ISI laser light is presented. A direct measurement of the self-focusing growth length has been made and compared with analytical model predictions. In addition, the possibility of inhibited radial thermal transport, strongly suggested in the observations, and its effect on the self-focusing are also discussed. Further, the backscattered levels of the Brillouin and Raman instabilities, also monitored, revealed that the effectiveness of the ISI in suppressing such instabilities becomes severely degraded when laser self-focusing occurs.

The preformed plasma was generated by exploding aluminum stripe targets [7,8]. Two pairs of opposing broadband laser beams ($\lambda_0 = 0.53$ μm, FWHM $= 600$ ps, $\Delta\omega/\omega = 0.1\%$), each smoothed using ISI in combination with a random-phase plate, irradiated the target surface using line-focus optics. The size of the line focus at the FWHM intensity (length, 0.8 mm; width, 0.4 mm) was larger than the target surface. A broadband infrared beam ($\lambda_0 = 1.06$ μm, FWHM $= 600$ ps, $\Delta\omega/\omega = 0.1\%$, $t_c = 3$ ps), smoothed by ISI alone, was delayed ($t_D = 1.7$ ns) with respect to the "heating" beams and used to interact with the preformed plasma column along its longitudinal axis (i.e., perpendicular to the direction of the heating beams) [3,8]. An aspheric $f/10$ lens was used to couple the beam into the plasma (focal-spot size, 140 μm at FWHM) located in the far field of the lens. Assuming a roughly planar hydrodynamic expansion for the relatively large foil targets irradiated, a 1D self-similar model was used to estimate the plasma state [7]. In particular, the transverse plasma scale length generated is of the order of $L_n \simeq 550$ μm at $t_D = 1.7$ ns. This is sufficiently large with respect to the interaction-beam focal spot that refraction effects can be neglected, and is consistent with experimental observations [3]. An array of plasma diagnostics has been used to characterize the plasma density and temperature conditions. These included time-resolved spectral analysis of (i) the plasma x-ray emission and (ii) the backscattered stimulated Brillouin (B-SBS) and Raman (B-SRS) signals. A fast calibrated photodiode and an energy calorimeter were used to measure the B-SBS energy level [9]. A spectrally filtered calibrated photodiode (germanium detector) was used to detect the presence of any B-SRS in the 1.4–2-μm emission

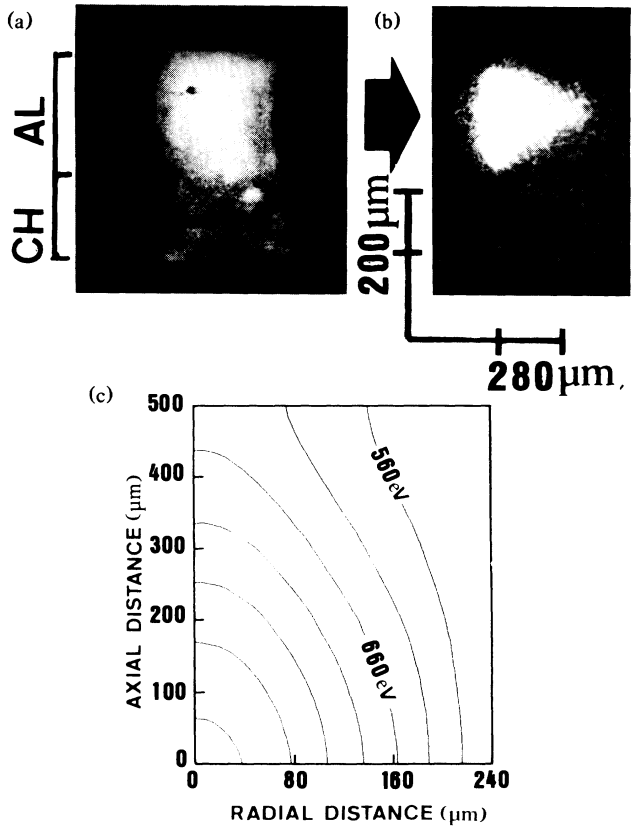

FIG. 1. A typical laser-plasma interaction record where no significant self-focusing is detected. (a),(b) A time sequence of x-ray framing images (140 ps gate time) of the preformed plasma 1 ns before the start of the pulse and 50 ps before the peak of the pulse, respectively. The interaction delay $t_D = 1.7$ ns with $N_e \simeq 0.3 N_c$ and $T_e \simeq 500$ eV. Average irradiance $I_{av} = 3 \times 10^{14}$ W cm^{-2}; focal-spot size, 140 μm. The direction and spatial location of the interaction beam is indicated by the arrow in (a). The heating beams are directed normal to the plane of the paper (i.e., perpendicular to interaction beam). The CH-Al brackets indicated in (a) approximately locate the original plastic-aluminum boundaries. (c) A 2D simulation of the average temperature distribution during the gating period (140 ps gate time) of the framing-camera gating (190 to 50 ps before the peak of the pulse) to model the record in (b). The contour interval is 50 eV.

range, using interference filters (bandwidth FWHM, 0.1 μm). A four-channel pinhole camera (10-μm-diam pinholes, 3-μm-thick Al filter) coupled to a four-channel x-ray framing camera (140 ps gate time) provided a time sequence of x-ray images of the laser-plasma interaction. In addition, uv probing ($\lambda_p = 350$ nm, FWHM = 70 ps) with a moiré deflectometer [10] system normal to the direction of the interaction beam was used to reveal induced transverse density gradients ($\partial N_e / \partial y$) in the preformed plasma by mapping the refraction profile of the probe beam [sensitivity, 0.56 mrad/(fringe shift)].

Figure 1 shows a sequence of two x-ray framing images (140 ps gate time) of the preformed plasma. Figure 1(a) is recorded with the gating period ending 1 ns before the arrival of the interaction pulse and Fig. 1(b) is recorded with the gating period ending 50 ps before the peak of pulse. The aluminum stripe was 700 nm thick, 0.5 mm long, and 0.3 mm wide and supported on a 100-nm-thick Formvar substrate. The total heating irradiance is $I_H \simeq 10^{14}$ W cm^{-2}. The average interaction irradiance is $I_{av} = 3 \times 10^{14}$ W cm^{-2}. Early in its evolution the electron temperature is sufficiently high ($T_e > 1$ keV) for the preformed plasma to be imaged directly via its thermal emission, as shown in Fig. 1(a). The fractional transmission of the 3-μm Al filter is $T_r \simeq 0.5$ at $T_e \simeq 1$ keV. At $t_D = 1.7$ ns, the measured plasma electron density and temperature are $N_e \simeq 3.2 \times 10^{20}$ cm^{-3} and $T_e \simeq 500$ eV, respectively. The background plasma emission is now too weak to be readily detected ($T_r = 0.01$ for $T_e = 500$ eV). As such, this enables the propagation characteristics of the interaction beam to be readily differentiated by its localized reheating of the plasma, as shown in Fig. 1(b). In Fig. 1(c), a 2D simulation of the average temperature distribution caused by the heating of the interaction beam during the gating time of the framing camera is presented. We have assumed linear inverse-bremsstrahlung absorption and classical electron thermal transport. The strong localized on-axis heating recorded in Fig. 1(b) would appear to be characteristic of the temperature distribution expected under normal interaction conditions, and cannot be attributed to laser self-focusing.

Figure 2 shows a sequence of three x-ray framing images of the preformed plasma taken with the gating period of the framing camera ending 1 ns before the interaction, 50 ps before the peak of the pulse, and 150 ps after the peak of the pulse, respectively. The interaction irradiance is $I_{av} = 2.5 \times 10^{14}$ W cm^{-2}. In contrast to the interaction conditions of Fig. 1, the target thickness and heating irradiance were adjusted to produce a more collisional interaction while still allowing for a direct comparison to be made between the two interaction conditions. This was achieved by exploding a thinner Al foil target (500 nm thick, 0.35 mm long, 0.3 mm wide) with a reduced heating irradiance $I_H = 3.5 \times 10^{13}$ W cm^{-2}. The effect was to produce a preformed plasma with a virtually unchanged peak (on-axis) electron density but with a significantly reduced electron temperature at $t_D = 1.7$ ns, i.e., 63% of the previous value [7]. This value was consistent with the measured plasma temperature $T_e \simeq 300$ eV. The effect is to enhance the strength of the thermal self-focusing mechanism (γ_{TF}) which is strongly temperature dependent, $\gamma_{TH} \sim T_e^{-5} (N_e/N_c)^2$ [11].

Inspection of Figs. 1 and 2 clearly shows that at the input, the interaction beam causes strong local heating. A clear contrast is evident in the propagation characteristics of the interaction beam between the two interaction regimes. A strong filamentory channel has formed in Figs. 2(b) and 2(c) about 200 μm from the plasma input plane, with a transverse scale length (≤ 50 μm) less than the beam diameter. At the exit plane we also observe a

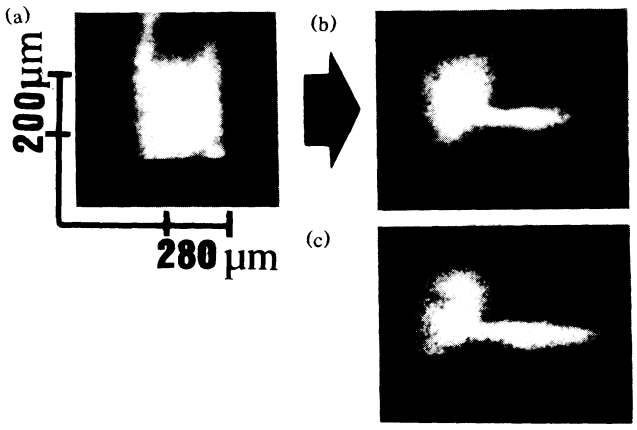

FIG 2. A time sequence of x-ray framing images (140 ps gate time) recording the preformed plasma (a) 1 ns before the start of the pulse, (b) 50 ps before the peak of the pulse, and (c) 150 ps after the peak of the pulse. The interaction-beam delay $t_D = 1.7$ ns with $N_e \simeq 0.3 N_c$ and $T_e \simeq 300$ eV. The direction of the interaction beam is indicated by the arrow in (a). The average interaction irradiance $I_{av} = 2.5 \times 10^{14}$ W cm^{-2}; focal-spot size, 140 μm. A strong emission channel is clearly identified in (b) and (c), consistent with beam self-focusing.

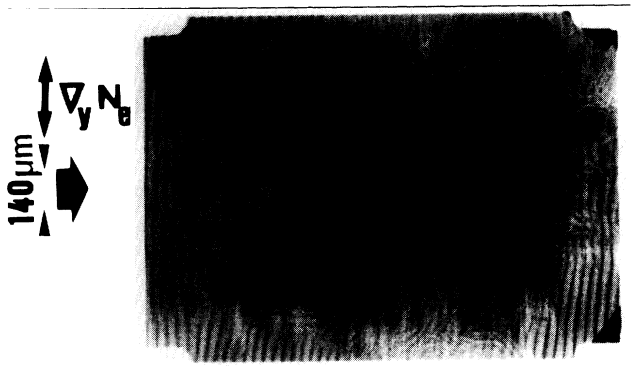

FIG. 3. A morié deflectometer data record of the preformed plasma taken at the end of the interaction pulse under similar plasma conditions as in Fig 2, with $I_{av} = 4 \times 10^{14}$ W cm^{-2}. Strong local plasma heating caused by the interaction beam is clearly evident with the formation of a density cavity at the input. The radial dimension of the cavity (with respect to the focal-spot size) and the fringe perturbations observed extending back towards the laser indicate that radial expansion and material ablation have contributed to the cavity formation. Strong density gradients ($\partial N_e/\partial_y$) are evident at the inner walls of the cavity indicated by the complete rotation to the horizontal of the fringes. There is also the indication of a filament channel formed at the apex of the cavity where the fringes also are strongly shifted.

strong emission plume extending beyond the exit, which is consistent with hot plasma being expelled from a filament channel by the beam breakout. Further confirmation of some of these features is provided in Fig. 3, where a moiré deflectometer record under similar plasma conditions as in Fig. 2 is shown. The interaction irradiance is $I_{av} = 4 \times 10^{14}$ W cm^{-2}. The probe beam was timed to arrive at the end of the interaction pulse. The effects of the strong plasma heating are clearly evident causing both radial expansion as well as ablation from the heated region back towards the laser as detected by the perturbations caused in the moiré fringes.

Also particularly relevant is the contrast between the levels of B-SBS and B-SRS recorded for the two interaction regimes presented. The B-SBS fraction (E_{SBS}%) measured for the interaction in Fig. 1 was $E_{SBS} = 0.3\%$ [9]. For the interaction in Fig. 2, the B-SBS level was around an order of magnitude greater ($E_{SBS} = 2\%$), nearing the saturation level recorded with non-ISI interactions ($E_{SBS} \simeq 4\%$) [9]. A fivefold increase was also recorded in the relative magnitude of the B-SRS signal. The peak B-SRS emission occurred at $\lambda_{SRS} \simeq 1.55$ μm (FWHM $= 0.1$ μm), which suggests that the emission is emanating from density regions of around $0.1 N_c$ [8], well below the background density.

For the large-scale-length intensity modulation presented by the focal spot size ($\lambda_\perp = 140$ μm) thermokinetic pressure is expected to initiate whole-beam self-focusing. For our conditions, $N_e/N_c = 0.3$, $Z = 13$, and $\ln\Lambda = 7$ (the Coulomb logarithm), the thermal filamentation spatial growth rate is

$$G^{TF}(\mathrm{m}^{-1}) \simeq 5.92 \times 10^6 [0.21 \gamma_{TF} - (\lambda_0/\lambda_\perp)^4]^{0.5}$$

(see Table I of Ref. [11]), where $\gamma_{TF} \simeq 2.48 \times 10^{-6} \times I_0 (10^{14}\ \mathrm{W\,cm^{-2}}) T_e(\mathrm{keV})^{-5}$. The growth (or focusing) length is $L_f \simeq 1/G^{TF}$. For the interaction conditions ($T_e = 500$ eV, $I_0 = 3 \times 10^{14}$ W cm^{-2}) in Fig. 1, G^{TF} is sufficiently strong to cause self-focusing in a distance $L_f \simeq 24$ μm. Here, the ratio of thermal to ponderomotive growth rates is $G^{TF}/G^{PF} \simeq 8{:}1$. For the cooler plasma conditions in Fig. 2 ($T_e \simeq 300$ eV, $I_{av} = 2.5 \times 10^{14}$ W cm^{-2}), G^{TF} is increased by approximately threefold to give $L_f \simeq 7$ μm, with $G^{TF}/G^{PF} \simeq 21{:}1$. The time scale for the self-focusing is of the order of the ion-acoustic transit time $t_h \simeq \lambda_\perp / 2c_s$. For $\lambda_\perp = 140$ μm, then $t_h \simeq 400$ ps. However, it should be noted that although the filamentation theory can provide an indication for when conditions become favorable to thermal whole-beam self-focusing, it generally overestimates the spatial growth rate. The theory assumes only small plasma perturbations, not strictly valid for our conditions as both plasma density and temperature are expected to be significantly modified. As such, it is instructive to compare these predictions with a simple model [12], where these parameters are treated self-consistently, although the model has been applied to a coherent beam interaction with a parabolic spatial profile. The self-focusing length is given by

$$L_f \simeq 5 r_0 (N_c/N_e)^{0.5} A^{-0.5} (1 + 0.6A)^{0.57},$$

where

$$A \simeq \frac{9.3 \times 10^{-39} r_0(\mathrm{cm})^2 \lambda_0(\mu\mathrm{m})^2 I_0(\mathrm{W\,cm^{-2}}) Z^2 N_e(\mathrm{cm^{-3}})^2}{T_e(\mathrm{eV})^5}$$

and r_0 is the initial beam radius (at FWHM). For our

conditions with $N_e/N_c=0.3$, $T_e=500$ eV, and $I_0=3\times10^{14}$ W cm^{-2} the focusing length is increased by around 27-fold to $L_f\simeq660$ μm. As such, we can expect only partial whole-beam self-focusing for these conditions and can explain why strong self-focusing was not recorded in Fig. 1. Unfortunately, the model tends to overestimate L_f values for lower temperatures (see Fig. 3 of Ref. [12]). Nonetheless, assuming a similar 27-fold increase in L_f from that predicted by filamentation theory suggests that $L_f\simeq190$ μm, which compares well with the measured growth length $L_f\simeq200$ μm, from Fig. 2.

This correlation might well be fortuitous since many simplifying assumptions have been made in the model. A more detailed description would require the effect of plasma absorption be included, since this would act directly to reduce G^{TF} by attenuating the beam intensity. On the other hand, the inclusion of ponderomotive forces and in particular transverse plasma flow [13] can both significantly increase G^{TF}. However, the description of thermal energy transport is probably the biggest uncertainty in the modeling of laser self-focusing. Recently, the linear theory for thermal self-focusing has been extended to include the effects of nonlocal heat transport [14]. The resulting inhibition of heat flow allows for higher temperature, density, and refractive-index modulations which substantially reduces the threshold of the instability and gives rise to an optimum perturbation wavelength that maximizes the spatial growth. To take account of kinetic transport effects the conductivity can be modified to $K=K_{\mathrm{SH}}[1+(30k_\perp\lambda_e)^{4/3}]^{-1}$, where K_{SH} is the classical Spitzer-Harm conductivity,

$$\lambda_e(\mu\mathrm{m})\simeq40[T_e(\mathrm{keV})^2\lambda_0(\mu\mathrm{m})^2N_c/N_e]/\ln\Lambda(Z+1)^{1/2}$$

is the electron stopping length, and $k_\perp=2\pi/\lambda_\perp$ is the perturbation wave number. The criterion for kinetic effects to dominate is that $\lambda_\perp<\lambda_c=60\pi\lambda_e$. For our initial interaction conditions $N_e/N_c=0.3$, $T_e=500$ eV, $\lambda_0=1.06$ μm, and $Z=13$ we have $\lambda_c=264$ μm. As such, the kinetic regime may be valid for our interaction since the beam focal spot $\lambda_\perp=140$ μm $<\lambda_c$. For the perturbation wavelength $\lambda_\perp=140$ μm, $K\simeq0.3K_{\mathrm{SH}}$. This suggests a factor-of-3 reduction in the radial conduction rate for the initial interaction region. The effect will be to enhance G^{TF} by increasing $\gamma_{\mathrm{TF}}\rightarrow\gamma_{\mathrm{TF}}/0.3$. Similarly, for a filament channel with $\lambda_\perp=30$ μm, $K\simeq0.05K_{\mathrm{SH}}$.

A characteristic thermal diffusion length $L_D(\mathrm{cm})\simeq[K_{\mathrm{SH}}t/N_e]^{1/2}$ in a time t (s) can be determined from the 1D thermal transport equation. This suggests that the heat should diffuse to $L_D\simeq140$ μm in 200 ps assuming classical thermal transport. Similarly, this should increase to $L_D\simeq340$ μm when $T_e=1$ keV, suggesting that classical thermal transport would significantly broaden the heated plasma region. This suggests that thermal imaging should provide only limited information concerning the propagating behavior of the interaction beam, contrary to the images presented in Figs. 2(b) and 2(c) (time interval $\simeq200$ ps). However, if we assume a flux-inhibited flow the broadening will be significantly reduced and provides an explanation of the data. The thermal diffusion length will now reduce to $L_D\simeq50$ μm for $\lambda_\perp=140$ μm, with $T_e=500$ eV. For the self-focusing region $L_D\simeq7$ μm for $\lambda_\perp=30$ μm, and even at $T_e=1$ keV the diffusion length is still not more than half the perturbation radius for the self-focused channel.

In conclusion, clear evidence has been obtained of thermal whole-beam self-focusing of ISI laser light in large underdense plasmas. The self-focusing growth length, and its dependence on the experimental conditions, appears to be reasonably well explained by classical thermal self-focusing. However, the results strongly suggest that the effects of nonlocal heat transport may also have played an important role in enhancing the thermal self-focusing mechanism. As such, this may pose a serious problem for the implementation of ISI on larger multikilojoule laser systems, and the current trend towards laser irradiation with shorter wavelengths (since $G^{\mathrm{TF}}\sim[(N_e/N_c)\gamma_{\mathrm{TF}}]^{1/2}$, where $\gamma_{\mathrm{TF}}\sim I_0Z^2N_e^2\lambda_0^4T_e^{-5}$). We note that the resulting increase in absorption will eventually compete with self-focusing to reduce its effect, but only for extremely collisional interaction conditions [6]. However, a possible method to counter the instability, which warrents further investigation, is to produce a more broadened ISI spatial profile at the focal plane, rather than the sinc^2 function produced by the square ISI echelon steps used here [15].

We wish to acknowledge the support of the laser group of the Rutherford Appelton Laboratory where this experiment was carried out.

[1] M. H. Emery *et al.*, Phys. Rev. Lett. **48**, 253 (1982).
[2] D. Havazelet *et al.*, Phys. Fluids B **1**, 893 (1989).
[3] O. Willi *et al.*, Phys. Fluids B **2**, 1318 (1990).
[4] R. H. Lehmberg and S. P. Obenschain, Opt. Commun. **46**, 27 (1983).
[5] S. P. Obenschain *et al.*, Phys. Rev. Lett. **62**, 768 (1989); S. E. Coe *et al.*, Europhys. Lett. **10**, 31 (1989); A. N. Mostovych *et al.*, Phys. Rev. Lett. **59**, 1193 (1987).
[6] R. D. Jones *et al.*, Phys. Fluids **31**, 1249 (1988); S. E. Coe, T. Afshar-rad, and O. Willi, Europhys. Lett. **13**, 251 (1990).
[7] R. A. London and M. Rosen, Phys. Fluids **29**, 3813 (1986).
[8] O. Willi *et al.*, Opt. Commun. **70**, 487 (1989).
[9] T. Afshar-rad *et al.* (unpublished).
[10] O. Kafri and J. Krasinski, Appl. Opt. **24**, 2746 (1985).
[11] A. J. Schmitt, Phys. Fluids **31**, 3079 (1988).
[12] K. Estabrook, W. L. Kruer, and D. S. Bailey, Phys. Fluids **28**, 19 (1985).
[13] A. J. Schmitt, Phys. Fluids B **1**, 1287 (1989).
[14] E. M. Epperlein, Phys. Rev. Lett. **65**, 2145 (1990).
[15] A. J. Schmitt and J. H. Gardner, J. Appl. Phys. **60**, 6 (1986).

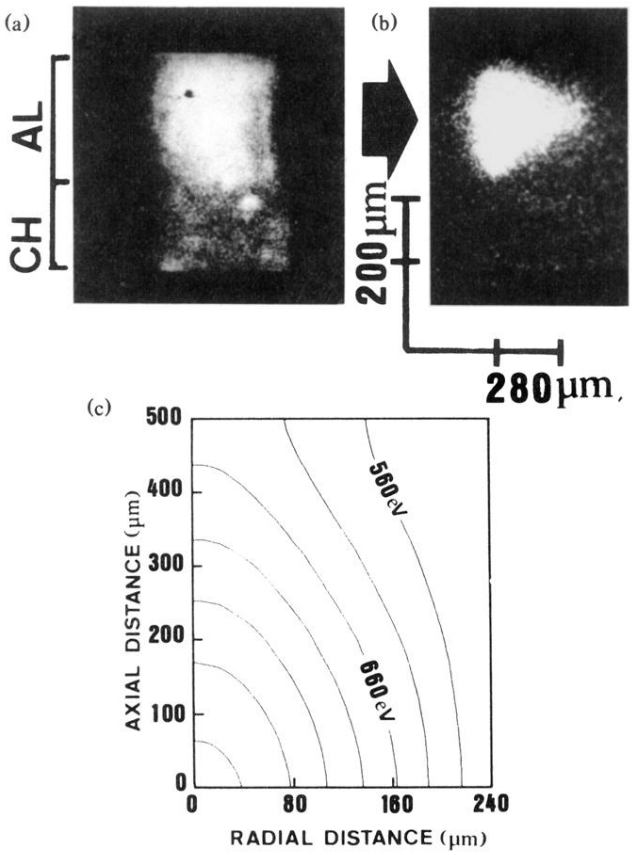

FIG. 1. A typical laser-plasma interaction record where no significant self-focusing is detected. (a),(b) A time sequence of x-ray framing images (140 ps gate time) of the preformed plasma 1 ns before the start of the pulse and 50 ps before the peak of the pulse, respectively. The interaction delay $t_D = 1.7$ ns with $N_e \simeq 0.3 N_c$ and $T_e \simeq 500$ eV. Average irradiance $I_{av} = 3 \times 10^{14}$ W cm^{-2}; focal-spot size, 140 μm. The direction and spatial location of the interaction beam is indicated by the arrow in (a). The heating beams are directed normal to the plane of the paper (i.e., perpendicular to interaction beam). The CH-Al brackets indicated in (a) approximately locate the original plastic-aluminum boundaries. (c) A 2D simulation of the average temperature distribution during the gating period (140 ps gate time) of the framing-camera gating (190 to 50 ps before the peak of the pulse) to model the record in (b). The contour interval is 50 eV.

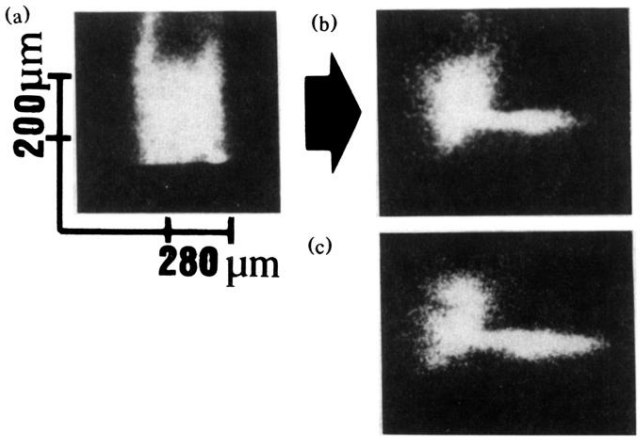

FIG 2. A time sequence of x-ray framing images (140 ps gate time) recording the preformed plasma (a) 1 ns before the start of the pulse, (b) 50 ps before the peak of the pulse, and (c) 150 ps after the peak of the pulse. The interaction-beam delay $t_D = 1.7$ ns with $N_e \simeq 0.3 N_c$ and $T_e \simeq 300$ eV. The direction of the interaction beam is indicated by the arrow in (a). The average interaction irradiance $I_{av} = 2.5 \times 10^{14}$ W cm^{-2}; focal-spot size, 140 μm. A strong emission channel is clearly identified in (b) and (c), consistent with beam self-focusing.

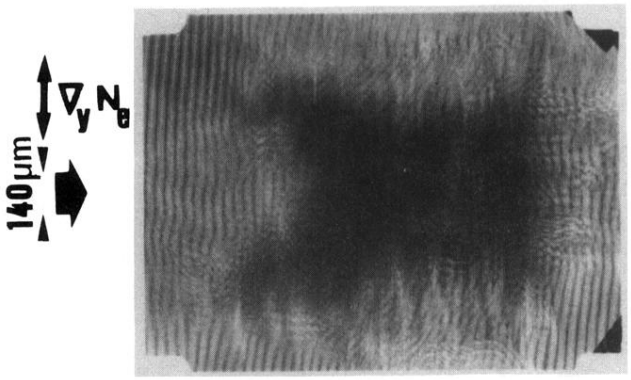

FIG. 3. A morié deflectometer data record of the preformed plasma taken at the end of the interaction pulse under similar plasma conditions as in Fig 2, with $I_{av}=4\times10^{14}$ W cm^{-2}. Strong local plasma heating caused by the interaction beam is clearly evident with the formation of a density cavity at the input. The radial dimension of the cavity (with respect to the focal-spot size) and the fringe perturbations observed extending back towards the laser indicate that radial expansion and material ablation have contributed to the cavity formation. Strong density gradients ($\partial N_e/\partial_y$) are evident at the inner walls of the cavity indicated by the complete rotation to the horizontal of the fringes. There is also the indication of a filament channel formed at the apex of the cavity where the fringes also are strongly shifted.